Pressure Effects on Lipidic Direct Phases: The Dodecyl Trimethyl Ammonium Chloride−Water System

Lydia Paccamiccio,[†] Michela Pisani,[‡] Francesco Spinozzi,[†] Claudio Ferrero,[§] Stephanie Finet,[§] and Paolo Mariani*,[†]

Dipartimento di Scienze Applicate ai Sistemi Complessi, Università Politecnica delle Marche, Via Ranieri 65, I-60131 Ancona, Italy, Dipartimento di Scienze dei Materiali e della Terra, Università Politecnica delle Marche, Via Brecce Bianche, I-60131 Ancona, Italy, and European Synchrotron Radiation Facility, BP 220, F-38043 Grenoble Cedex, France

The direct lyotropic polymorphism of dodecyltrimethylammonium chloride (DTAC) was investigated by synchrotron X-ray diffraction at different water concentrations under compression up to 2 kbar, i.e., in the pressure intermediate range where interesting biophysical transformations occur and the functional characteristics of cell membranes are altered. The results show that pressure induces the transition from the hexagonal phase to the micellar $Pm3n$ cubic phase in hydrated samples (c between 0.5 and 0.6, c being the weight concentration of lipid in the mixture) and the transition from the bicontinuous $Ia3d$ cubic phase to the hexagonal phase in drier samples ($c = 0.8$). By increasing the pressure on very dry samples, a lamellar L_α phase was observed to form transitorily at the $Ia3d$ cubic−hexagonal phase transition. Phase compressibility and then the lipid and water partial molecular compressibilities were derived as a function of pressure and concentration. As a result, we assessed the very low compressibility of the hydration water within the lipid phases, and we demonstrated that the compressibility of DTAC is very dependent on pressure. Moreover, the molecular parameters of DTAC calculated in the different phases during compression confirmed that pressure induces small but continuous conformational changes, definitely different from the large changes observed in lipid molecules forming type II structures.

I. Introduction

Over the past decade, the application of hydrostatic pressure has become an interesting tool for analyzing structural properties and phase behavior of biological molecules and systems.[1,2] In particular, quite relevant are studies at intermediate pressures, as the range where interesting biophysical transformations occur (like protein denaturation, oligomer dissociation, helix-coil transition in nucleic acids, bacteria inactivation) is typically 0.1−0.5 GPa and very rarely up to 1 GPa (pressures in the range from 1 to several kilobars are called medium or intermediate pressures. 1 kbar = 0.1 GPa).[3]

In this context, remarkable results have been obtained in inverse (type II, water-in-oil) lipid systems. A number of different phase transitions was observed to occur at intermediate pressures, as, for example, the hexagonal-to-lamellar phase transition detected in hydrated dioleyl phosphatidyl ethanolamine[4−6] and the cubic-to-cubic and cubic-to-lamellar phase transitions detected at different concentrations in the monolein/water system.[7−9] Moreover, the unit cell compressibility in the inverse phase has been firmly established to be negative (i.e., pressure induces an increase of the unit cell dimension).[4−9] However, the pressure dependence of the lattice constants was observed to be larger for structures occurring in excess of water.[4,6,9] Simple molecular packing arguments, based on pressure-induced changes in the basic geometrical wedge shape of the lipid molecules, were exploited to account for these

features,[8,10] but a change in the hydration level was also associated to the shape variation.[4,6,9]

In inverse lipid systems, structural data obtained in the biologically relevant range were also helpful to derive information on the stability of the lipid layer.[6,8,9] Using a free energy model based on curvature elastic contributions, we demonstrated that in monoolein the monolayer spontaneous curvature tends to zero when the pressure increases, but we argued that the bending elasticity is not prevailing in the total free energy of the system under compression.[8,9] More recently,[6] we reported that the isothermal lateral compression constant in dioleyl phosphatidyl ethanolamine monolayer is practically independent of concentration, while it increases as a function of pressure. Howerver, changes in the bending rigidity and spontaneous curvature of the monolayer suggested that, as the pressure increases, the lipid chain repulsion becomes relatively weaker, and thereby less efficient in balancing the torque of headgroup repulsion.

Owing to their topology, medium-pressure effects on direct (type I, oil-in-water) lipid phases are expected to be quite different from those observed in inverse phases. However, direct systems have been only sparingly investigated.[1] Structural investigations in the pressure range 0.001−4 kbar concerned, for example, the critical micelle concentration (cmc) of ionic and nonionic surfactants in aqueous solutions.[1,11] The initial compression was observed to cause the dissociation of micelles, whereas successive compression above a certain pressure causes aggregation of monomers to micelles again, suggesting that the partial molecular volume change on micellation is positive in the lower pressure region and negative for the higher pressures.

[†] Dipartimento di Scienze Applicate ai Sistemi Complessi.
[‡] Dipartimento di Scienze dei Materiali e della Terra.
[§] European Synchrotron Radiation Facility.
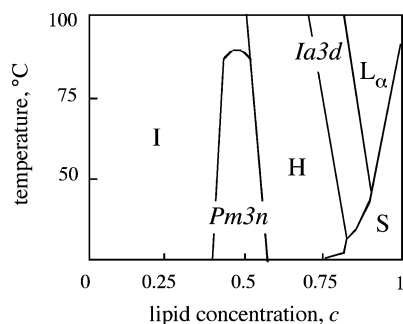
Figure 1. Temperature−concentration dependent phase diagram of the DTAC/water system at atmospheric pressure (redrawn from Balmbra et al.[13]). S, crystal; L_α, lamellar; *Ia3d*, direct bicontinuous cubic of *Ia3d* symmetry; H, direct hexagonal; *Pm3n*, direct micellar cubic of *Pm3n* symmetry; I, isotropic fluid.

The similar characteristic pressure dependence of the cmc for both ionic and nonionic surfactants, as well as the existence of an alkyl chain length dependence for ionic surfactants, suggested that the effect of pressure is largely independent of the hydrophilic headgroup of the surfactant.[1] Concentrated micellar systems and microemulsions were also analyzed under compression, and changes in aggregation number and the formation of aggregate structures with smaller partial molecular volumes of their amphiphiles were revealed.[1] In some cases, pressure-induced phase transitions from droplet structures or from rodlike micelles to lamellar phases were also detected.[1,12] These data clearly indicate that already relatively low pressures can lead to drastic changes in structure and topology of type I lipid systems.[1]

In this work, we extend high-pressure structural investigations to concentrated lipid systems, considering the special case of the dodecyltrimethylammonium chloride (DTAC) in water, which exhibits an extended direct lyotropic polymorphism at atmospheric pressure.[13,14] The temperature−concentration dependent phase diagram of DTAC is shown in Figure 1: it can be observed that the central region is characterized by the presence of a direct hexagonal H phase, while a micellar *Pm3n* cubic phase extends between the hexagonal and the isotropic fluid phases, and a *Ia3d* bicontinuous cubic phase occurs in the drier side of the phase diagram. Furthermore, in the very dehydrated conditions, a lamellar liquid crystalline phase exists. The schematic representation of the lyotropic phases occurring in the DTAC/water system is reported in Figure 2. The *Pm3n* cubic phase is the first example among lipids of a structure containing elements of more than one form.[14−16] Its structure consists of two types of disjointed micelles of type I, embedded in a continuous water matrix. The eight micelles contained in the unit cell belong to two different classes: two are globular and located at the corner and in the center of the cubic cell (referred to as positions **a**), while six are disk-shaped and located on the cell faces at positions **c**.[15] Since the lipid component is chemically homogeneous, it was concluded that the area per molecule values are the same in the two types of micelles.[14,15] The hexagonal H phase consists of a hexagonal array of infinitely long cylinders, filled by the hydrocarbon chains, coated with the DTAC polar headgroups, and embedded in the water matrix.[17] The *Ia3d* cubic phase is bicontinuous and can be described in terms of two three-dimensional (3D) networks of joined rods, mutually intertwined and unconnected.[14,17] The rods are filled by the hydrocarbon chains, have equal length, and are 3 × 3 coplanarly joined.

In the present study, the polymorphism of DTAC at intermediate pressures was analyzed by synchrotron X-ray diffraction
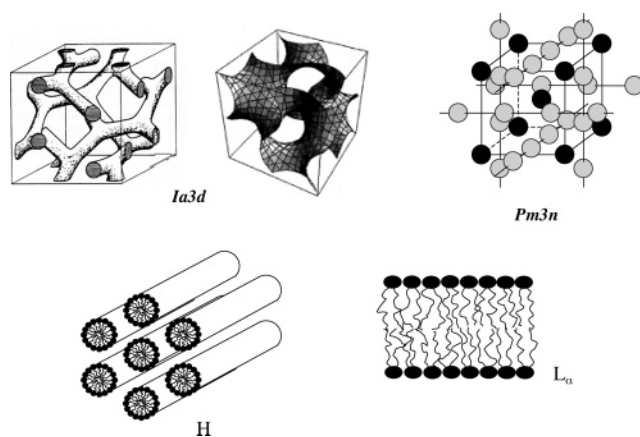
Figure 2. Schematic representation of the phases observed in the DTAC/water system. Symbols as in Figure 1. For the *Ia3d* cubic phase, the *G* minimal surface, which locates the midplane of the aqueous region,[16] is also shown. For the *Pm3n* cubic phase, black and gray spheres indicate the points where the different types of micelles (**a** and **b**, respectively; see text) are centered.

at water concentrations ranging from 40 to 90 weight lipid % under hydrostatic pressures up to 2 kbar.

II. Materials and Methods

DTAC (99.0% purity) was obtained from Sigma Chemical Co. The DTAC/water system was analyzed in a concentration range spanning from $c = 0.45$ to $c = 0.90$. Samples were prepared by mixing the lipid with the required amounts of bidistilled water and were equilibrated for 1 day at ambient temperature and pressure. The relative concentration uncertainty was estimated to be 5%. No water loss was detected before the lipid mixtures were mounted into the pressure cell. Moreover, after the X-ray scattering experiments, the water composition of each sample was checked again by gravimetric analysis. The difference between the nominal concentration and the one measured after the pressure cycle was detected to be within the limit of the experimental error. The lipid volume concentration at ambient pressure was determined from the nominal weight composition c and the known specific volumes of the two components ($v_L = 1.103$ cm^3/g and $v_W = 1.0$ cm^3/g).

Diffraction experiments were performed at the ID02 beamline at the European Synchrotron Radiation Facility, ESRF, Grenoble (France), using a SAXS−WAXS setup.[6] The wavelength of the incident beam was $\lambda = 1$ Å, and the investigated Q-range was between 0.03 and 0.6 Å^{-1} ($Q = 4\pi \sin\theta/\lambda$, where 2θ is the scattering angle) on the SAXS detector and between 2.8 and 13.2 Å^{-1} on the WAXS detector. For high-pressure measurements, a NovaSwiss pressure-control system was used. The pressure cell has two diamond windows (3.0 mm diameter and 1 mm thickness) and allows measurement of diffraction patterns at hydrostatic pressures up to 3 kbar.

X-ray diffraction measurements were performed at 25 °C for different pressures, from 1 bar to about 2 kbar, with steps of about 100 bar. To avoid radiation damage, the exposure time was kept as low as 0.2−1 s/frame, and a fast beam shutter was used to protect the sample from irradiation when data were not being acquired. Particular attention was paid to checking for equilibrium conditions and monitoring radiation damage. Measurements were repeated several times (up to 10) at the same constant pressure to account for stability in position and intensity of the Bragg peaks. Accordingly, a gentle compression of the sample, at a rate of 0.5−2 bar/s, was sufficient to establish equilibrium conditions, including in the regions of phase
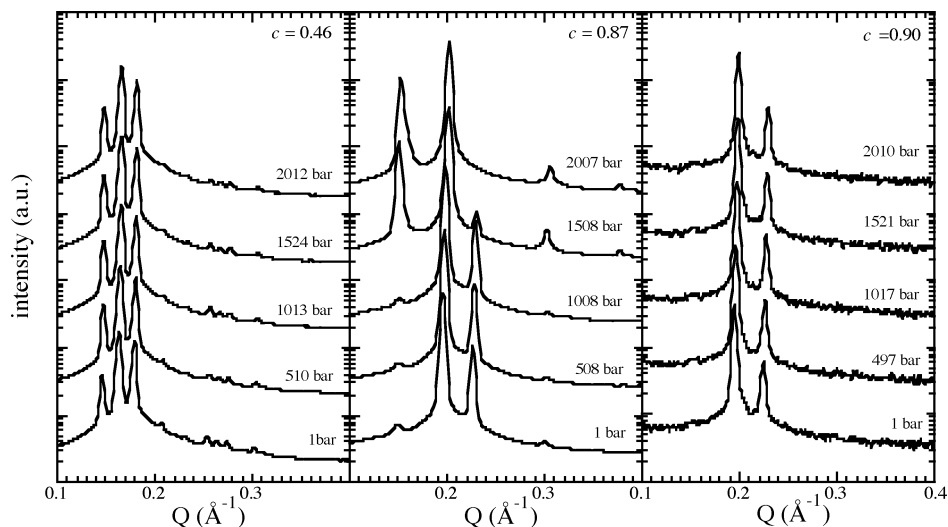
Figure 3. Low-angle X-ray diffraction profiles obtained at 25 °C from the DTAC/water system at concentrations of $c = 0.46$, $c = 0.87$, and $c = 0.90$; each experiment has been performed at the indicated pressures.

coexistence. In all cases, once the pressure got stabilized (within a few minutes), measurements were repeated at least twice, with a dead time of about 5 min. Since the scattering was isotropic, the data corrected for background, detector inhomogeneities, and sample transmission were radially averaged.

In each experiment, a number of sharp reflections were detected in the low-angle X-ray diffraction region and their spacings measured following the usual procedure.[14] SAXS profiles were indexed by considering the different symmetry systems commonly observed in lipid phases.[14,17] In particular, DTAC samples showed four different series of Bragg reflections, indexed according to the 1D lamellar symmetry (spacing ratios 1:2:3 ...), the 2D hexagonal space group (spacing ratios 1:$\sqrt{3}$:$\sqrt{4}$:$\sqrt{7}$ ...), the 3D *Pm3n* cubic space group (spacing ratios $\sqrt{2}$:$\sqrt{4}$:$\sqrt{5}$:$\sqrt{6}$:$\sqrt{8}$:$\sqrt{10}$ ...), and the 3D *Ia3d* cubic space group (spacing ratios $\sqrt{6}$:$\sqrt{8}$:$\sqrt{14}$:$\sqrt{16}$:$\sqrt{20}$:$\sqrt{22}$ ...). From the peak positions, the dimensions of the unit cell were calculated.

In the wide-angle region, a diffuse band was detected at all the investigated concentrations and pressures, indicating the disordered (type α) nature of the lipid short-range conformation.[17]

III. Results

X-ray diffraction experiments were performed at room temperature, at different water concentrations and pressures. Typical diffraction patterns are shown in Figure 3. In the low-angle region, 3 up to 10 peaks (depending on sample concentration) were observed. Under all the investigated conditions, the spacings of the peaks were unambiguously indexed. Even in the coexistence regions, the indexing problem was easy to solve, because no extra peaks, which can be ascribed to the presence of unknown phases or to crystalline structures, were observed.

A. Phase Diagram. The X-ray diffraction profiles indicate that pressure-induced phase behavior depends on sample composition. From the observed changes, the pressure−concentration phase diagram reported in Figure 4 has been derived. According to Figure 1,[13] the *Pm3n* cubic phase is detected in the more hydrated region (i.e., from $c = 0.4$ to $c = 0.5$). Under compression, diffraction data indicate a large stability of this phase, as no transition occurs up to 2 kbar. In the intermediate concentration region, from $c = 0.52$ to $c = 0.8$, the hexagonal phase is observed at ambient pressure.
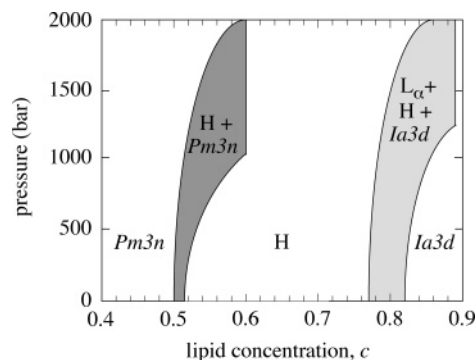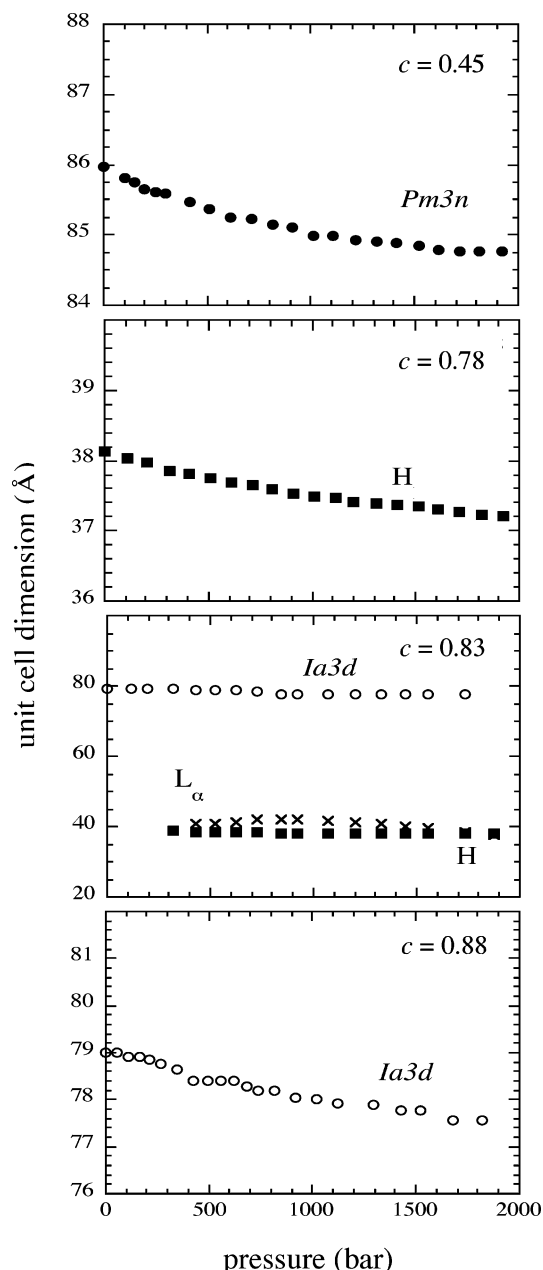

Figure 4. Pressure−concentration dependent phase diagram for the DTAC/water system at 25 °C. Symbols as in Figure 1. Phase coexistence regions are colored in gray.

However, in the more hydrated conditions (c between 0.52 and 0.58), the *Pm3n* cubic phase forms during compression. Noticeable is the fact that the cubic phase coexists with the H phase in a large pressure interval: as the intensities and positions of the diffraction peaks measured at constant pressure do not change as a function of time, while the intensities of the H characteristic peaks decrease as a function of pressure and the intensities of those related to the *Pm3n* phase increase, it can be concluded that the two phases are in a thermodynamic equilibrium.

At low hydration (from $c = 0.8$ to $c = 0.9$), the presence of the *Ia3d* cubic phase at ambient pressure is confirmed. X-ray diffraction profiles measured as a function of pressure point out that compression induces the transition to the H phase. However, it should be underlined that the pressure at which the transition occurs depends on concentration. In particular, the range of stability of the *Ia3d* cubic phase at high pressure increases with dehydration. Moreover, the *Ia3d*−H phase transition is accompanied by the formation of a transient lamellar phase. It is interesting to note that the lamellar phase forms a few hundred bars before the appearance of the H phase and disappears after the disappearance of the *Ia3d* cubic phase, suggesting that the transition is associated to local changes in sample composition.

Finally, in the drier samples ($c > 0.9$), the *Ia3d* cubic phase appears stable against pressure, even if the formation of a stable lamellar phase at $c = 0.95$ is stated at the high pressures.

B. Phase Compressibility. Unit cell dimensions were calculated from the positions of the diffraction peaks. A few
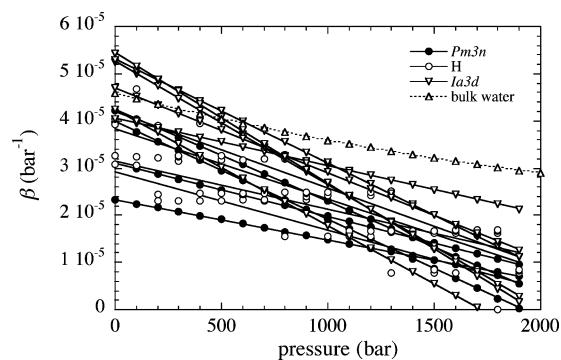
Figure 5. Pressure dependence of the unit cell dimensions of a few DTAC samples measured at 25 °C at different concentrations.

results are reported in Figure 5 to illustrate the general trend: in all cases, the unit cell shrinks during compression, even if the pressure dependence is very week. Note that the behavior observed in inverse phases was basically opposite: In both type II hexagonal and cubic phases, the unit cell dimensions were found to strongly increase under compression.[4−9]

A linear fit to the lattice dimensions measured on single phase domains served the purpose of calculating a rough value of the unit cell pressure dependence, da/dp. As it can be seen in Figure 6, da/dp depends on the structure of the phase and reduces within the same phase as the water content decreases. In particular, da/dp values range from about −0.6 to −0.7 Å kbar^{-1} in the *Pm3n* cubic phase, from −0.2 to −0.8 Å kbar^{-1} in the H phase, and from −1.0 to −1.2 Å kbar^{-1} in the *Ia3d* cubic phase. The comparison with the (positive) values of 1.3 Å kbar^{-1} and 1.0 Å kbar^{-1} observed in the lamellar phases of DOPE[6] and monolein,[6,9] respectively, or with the (positive) values of 1.6 Å kbar^{-1}, about 4 Å kbar^{-1}, and about 5−7 Å kbar^{-1} observed in
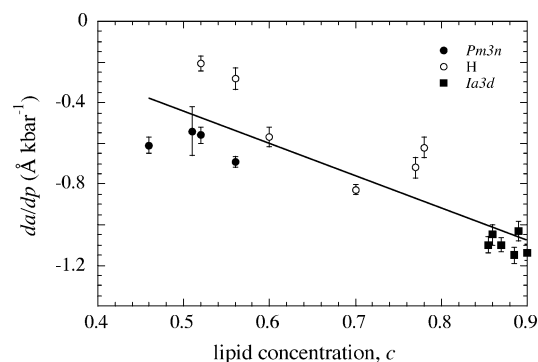
Figure 6. Concentration dependence of the lattice parameter variation per unit pressure, da/dp, at 25 °C. The straight line is only a guide to the eye.

Figure 7. Pressure dependence of the phase compressibility, β, of the *Pm3n*, H, and *Ia3d* phases for DTAC samples at 25 °C at different concentrations. For reference, the water compressibility (from ref 18) is also reported.

the DOPE inverse H phase and in the monoolein bicontinuous *Pn3m* and *Ia3d* cubic phases, respectively, clearly confirms that in direct lipid phases the pressure-induced behavior is definitively different.

The volume variations of the 2D hexagonal and 3D cubic phases under pressure were then used to derive the relative isothermal compressibilities. In the cubic phase, the isothermal compressibility is defined as the negative pressure derivative of the corresponding unit cell volume, V, at constant temperature

$$K_{T,3D} = \beta_{3D}V = -\left(\frac{\partial V}{\partial p}\right)_T \qquad (1)$$

where T is the absolute temperature, p the pressure, and $\beta_{3D} = -V^{-1}(\partial V/\partial p)_T$ the coefficient of 3D isothermal compressibility. In the hexagonal phase, information about the length of the cylinders cannot be obtained from data; therefore, the isothermal compressibility is defined as the negative pressure derivative of the area of the hexagonal primitive 2D cell at constant temperature, $\sigma = a^2\sqrt{3}/2$

$$K_{T,2D} = \beta_{2D}\sigma = -\left(\frac{\partial \sigma}{\partial p}\right)_T \qquad (2)$$

where $\beta_{2D} = \sigma^{-1}(\partial \sigma/\partial p)_T$ is the coefficient of 2D isothermal compressibility.

By visually inspecting the data, a quadratic dependence has been considered to calculate the pressure derivatives: β_{3D} and β_{2D} points are displayed in Figure 7, together with the coefficient of isothermal compressibility of the water[18] reported as reference. The isothermal compressibility coefficients of the three lipid phases are positive and decrease with pressure. Moreover, they are systematically lower than those of bulk water. Owing
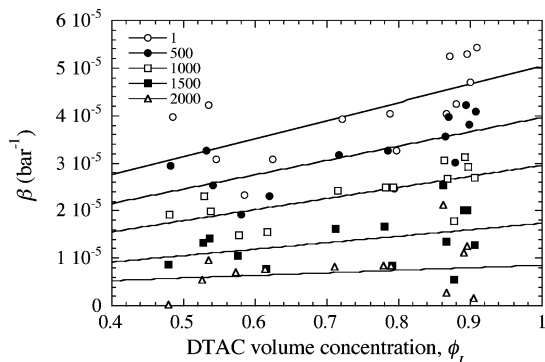
Figure 8. Volume concentration dependence of the phase compressibility, β, of the DTAC/water system at different selected pressures. Straight lines are the best fit curves obtained by analyzing the partial water and DTAC compressibilities (see text).

to the differences in the hydrogen bond networks in a confined space, water within the lipid phase appears to exhibit a compressibility (and hence a density) substantially different from the one characteristic of the bulk.

Figure 7 also show that the compressibilities in the various phases behave similarly, even if their values are clearly dependent on hydration. The concentration dependence of the coefficients of isothermal compressibility measured at constant pressure is reported in Figure 8 (as explained below, in this figure compressibility data are plotted as a function of the calculated pressure-dependent lipid volume concentration, ϕ_L, proportional to c). The points are scattered, but the general trend suggests that an increased hydration leads to a continuous decrease in compressibility, even when phase boundaries are crossed (the *Pm3n*−H phase transition occurs at ϕ_L around 0.58, while the H−*Ia3d* at about 0.82). Electrostriction of solvent around charged and polar groups could account for this behavior. We ought to observe that experimental results regarding the structure of the protein−water interface point to the existence of a first hydration shell with an average density 10% larger (and, as a possible consequence, a compressibility smaller) than that of bulk water.[19] The comparison with other studies suggested that this may be a general property of aqueous interfaces.[20]

C. Molecular Compressibility. According to the structural properties of a lipid phase, the partial DTAC and water compressibilities have been determined. Following Luzzati's model, it has been assumed that water is excluded from the regions where the hydrocarbon chains are clustered, while the hydrophilic groups of the lipid molecules cover the interface between the water and paraffin moieties.[17] The two topologically distinct volumes, corresponding to the lipid and aqueous moieties, are $V_L = \phi_L V$ and $V_W = (1 - \phi_L)V$, respectively. The net sample volume change induced by pressure, ΔV, can be then written as a sum of two components, ΔV_L and ΔV_W:[21] ΔV_L depends on the properties of the lipid moiety and includes the changes in the partial volume of the solute as well as any change in the interstitial volume owing to interactions of the solute with the solvent; ΔV_W arises from changes in the water partial volume.

The phase compressibility ($\beta = \beta_{3D} = \beta_{2D}$; see eqs 1 and 2) can be then related to the partial compressibility of the two components by

$$\beta = \phi_L \beta_L + (1 - \phi_L)\beta_W \qquad (3)$$

where β_L and β_W are the coefficients of isothermal partial compressibility of the lipid and water moieties, respectively (by

definition, β_L and β_W are also the isothermal partial molecular compressibility of the lipid and the water, respectively).

Due to the differences in the hydrogen bond networks in confined spaces, we expect that the compressibility of water confined in the lipid phase is different from that in the bulk. However, the situation could be more complicated in highly hydrated conditions, where only a fraction of the water directly interacts with the lipid polar surfaces. Consequently, β_W in eq 3 shoud be considered the average coefficient of isothermal partial (molecular) compressibility of the water in the lipid phase.

By means of an iterative analysis, β_L and β_W were derived from data in Figure 8. Following the original Tait equation (also known as linear secant modulus equation),[18,22] the pressure dependence of β_i can be described by a two-parameter equation

$$\beta_i(p) = \frac{\beta_i^\circ}{\left[1 + \frac{1}{2}\beta_i^\circ p(\eta_i + 1)\right]\left[1 + \frac{1}{2}\beta_i^\circ p(\eta_i - 1)\right]} \qquad (4)$$

where β_i° is the molecular compressibility at zero pressure and $\eta_i \equiv (\partial\beta_i^{-1}/\partial p)_{p=0}$ is the first derivative of the isothermal bulk modulus at the same pressure. Therefore, the pressure dependence of the molecular volume of the ith species can be obtained by integrating eq 4

$$v_i(p) = v_i^\circ\left[1 - \frac{\beta_i^\circ p}{1 + \frac{1}{2}(\eta_i + 1)\beta_i^\circ p}\right] \qquad (5)$$

(v_i° is the molecular volume at the zero pressure). This calculation is particularly relevant, as any change in lipid and water compressibility and volume reflects in changes of the sample volume concentration.

The approach has been the following: (i) compressibility data of Figure 8 were plotted as a function of the lipid volume concentration ϕ_L calculated at ambient pressure; (ii) a first set of coefficients of partial molecular compressibility, β_L and β_W, and the pair β_i° and η_i were derived by fitting data using eqs 3 4; (iii) the DTAC and water molecular volumes at different pressures were calculated from the pair β_i° and η_i by using eq 5. From molecular volumes, the lipid volume concentration was then calculated for each sample as a function of p; (iv) the compressibility data of Figure 8 were replotted as a function of the pressure-dependent lipid volume concentration and (v) these data were again fitted using eq 3 and eq 4 to obtain a new set of coefficients of partial molecular compressibility and a new pair β_i° and η_i. The procedure from steps (iii)−(v) was repeated until both water and DTAC partial compressibilities converged to stable values.

The lines reported in Figure 8 are the best fit curves to the compressibility data plotted as a function of the calculated pressure-dependent lipid volume concentration. The coefficients of isothermal partial molecular compressibility derived for DTAC and water molecules are reported as a function of pressure in Figure 9. As expected, water confined inside the lipid phase exhibits an unusually low compressibility, from 3 to 10 times lower than the compressibility observed in the bulk. Moreover, the DTAC compressibility appears to be heavily dependent on pressure: inasmuch as lipid compressibility represents a measure of intermolecular interactions, the observed behavior is arguably the signature of the tightness of intrinsic hydrocarbon packing induced by pressure.

The Compressibility of Water in the Lipid Phase: A Thermodynamical Model for Hydration. As previously dis-
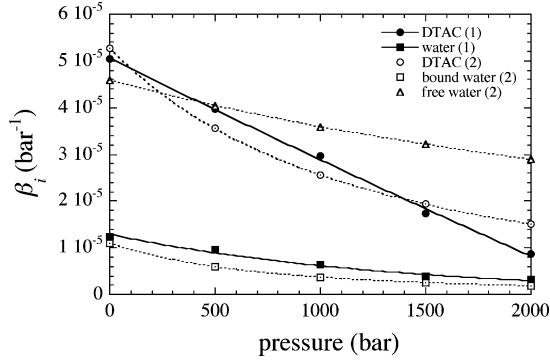
Figure 9. Pressure dependence of the partial DTAC and water compressibilities, β_i. Indices (1) and (2) refer to the values obtained from the two different analyses described in the text and based on eqs 3 and 6, respectively.

cussed, only a fraction of water could directly interact with the lipid polar surfaces in highly hydrated conditions. In terms of molecular properties, this implies that compressibility data in Figure 8 indeed contain, beyond the lipid contribution, compressibility contributions from water molecules which strongly interact with the lipid polar heads ("bound water", $W^{(B)}$) and contributions from water molecules which mainly behave as bulk water ("free water", $W^{(F)}$). Therefore, the isothermal phase compressibility, already defined in eq 3, should be written as a linear combination of the partial isothermal compressibilities of three components

$$\beta = \phi_L\beta_L + \phi_{W^{(B)}}\beta_{W^{(B)}} + \phi_{W^{(F)}}\beta_{W^{(F)}}$$
$$= \phi_L\beta_L + (1 - \phi_L)[\chi\beta_{W^{(B)}} + (1 - \chi)\beta_{W^{(F)}}] \qquad (6)$$

where χ is the volume fraction of bound water (defined with respect to the total aqueous volume).

   To determine the three compressibility contributions, a simple thermodynamical model for the lipid hydration has been resorted to. In particular, the process of hydration of the DTAC molecule (L) has been described by the equilibrium $LW_{j-1}^{(B)} + W^{(F)} \rightleftharpoons LW_j^{(B)}$, where j, the number of water molecules per lipid that strongly interact with the lipid polar surfaces, varies from 1 to N (by definition, N is then the maximum hydration number). In a simple approximation, the equilibrium constant K (and hence the corresponding Gibbs free energy variation, ΔG) can be assumed to be independent of j

$$K = \frac{[LW_j^{(B)}]}{[LW_{j-1}^{(B)}][W^{(F)}]} = e^{-\Delta G/k_B T} \qquad (7)$$

where T is the absolute temperature and k_B the Boltzmann constant, and the square brackets indicate the molar concentration of the different species. In its turn, ΔG depends on the chemical potentials of the different species. According to eqs 4 and 5, the chemical potentials of the ith species, μ_i, can be obtained by a successive integration of eq 5

$$\mu_i(p) = \mu_i^\circ + v_i^\circ$$
$$\left\{ \frac{(\eta_i + 1)(\eta_i - 1)\beta_i^\circ(p - p_0) + 4\log\left[\frac{\frac{1}{2}(\eta_i + 1)\beta_i^\circ p + 1}{\frac{1}{2}(\eta_i + 1)\beta_i^\circ p_0 + 1}\right]}{(\eta_i + 1)^2\beta_i^\circ} \right\}$$
$$= \mu_i^\circ + v_i^\circ f(p, \beta_i^\circ, \eta_i) \qquad (8)$$

In this equation, μ_i° is the chemical potential of the ith species at the reference pressure p_0 (1 bar, in the present case), and $f(p, \beta_i^\circ, \eta_i)$ represents the integral function between brackets. Therefore, ΔG can be written as

$$\Delta G = \mu_{LW_j^{(B)}} - \mu_{LW_{j-1}^{(B)}} - \mu_{W^{(F)}}$$
$$= \Delta G^\circ + v_{W^{(B)}}^\circ f(p, \beta_{W^{(B)}}^\circ, \eta_{W^{(B)}}) - v_{W^{(F)}}^\circ f(p, \beta_{W^{(F)}}^\circ, \eta_{W^{(F)}}) \qquad (9)$$

   As a unique value of K has been assumed, the reference free energy variation, $\Delta G^\circ = \mu_{LW_j^{(B)}}^\circ - \mu_{LW_{j-1}^{(B)}}^\circ - \mu_{W^{(F)}}^\circ$, does not depend on the hydration number j. Therefore, the pressure dependence of ΔG is only due to the differences between the standard volumes (v_i°) and compressibilities (β_i° and η_i) of the free and bound water molecules.

   The fraction of lipid molecules directly interacting with j water molecules can be calculated from eq 7 as

$$\alpha_j = \frac{[LW_j^{(B)}]}{C} = (K[W^{(F)}])^j \frac{1 - K[W^{(F)}]}{1 - (K[W^{(F)}])^{N+1}} \qquad (10)$$

where $C = n_L/VN_A$ is the molar concentration of lipid (N_A is Avogadro's number). By imposing the conservation of the total number of water molecules in the system, an implicit function of the bulk water concentration $[W^{(F)}] \equiv \phi_{W^{(F)}}/v_{W^{(F)}}N_A$ can be obtained

$$\frac{1 - c}{c}\frac{M_L}{M_W} = \langle j\rangle + \frac{v_L}{\phi_L}[W^{(F)}]N_A \qquad (11)$$

$$\langle j\rangle = \sum_{j=1}^{N}j\alpha_j \qquad (12)$$

$$\phi_L = \frac{cM_W v_L\{1 - [W^{(F)}]N_A(v_{W^{(F)}} - v_{W^{(B)}})\}}{c(M_W v_L - M_L v_{W^{(B)}}) + M_L v_{W^{(B)}}} \qquad (13)$$

where M_L and M_W are the molecular weight of DTAC and water, respectively. $\langle j\rangle$ represents the average occupation number (per lipid) of the water sites. The balance in eq 11 can be numerically solved in terms of $[W^{(F)}]$; $\langle j\rangle$, α_j, ϕ_L and χ can in turn be calculated and the compressibility of the mixture obtained through eq 6.

   The calculation of the coefficients of isothermal partial molecular compressibility is then performed by a global fit of data in Figure 8. The fit is based on eq 6 and on both the DTAC and water molecular volumes expressed as a function of pressure. Experimental conditions are labeled by the DTAC weight concentration, c, and the mechanical pressure, p. Fitting parameters are as follows: the reference volume, $v_{W^{(B)}}^\circ$, and the compressibility parameters of the hydration water, $\beta_{W^{(B)}}^\circ$ and $\eta_{W^{(B)}}$; the compressibility parameters of the DTAC, β_L° and η_L; the maximum number of hydration sites, N; the reference Gibbs free energy, ΔG°. The reference volumes of bulk water, $v_{W^{(F)}}^\circ$, and DTAC, v_L°, are considered to be known from density data at $p = 0$, while the compressibility parameters of bulk water at 20 °C have been set as $\beta_{W^{(F)}}^\circ = 4.59 \times 10^{-5}$ bar^{-1} and $\eta_{W^{(F)}} = 5.68$ from experimental compressibility data.[18]

   The numerical results are reported in Table 1, while the calculated coefficients of isothermal partial molecular compressibility for DTAC and bound water are plotted in Figure 9 as a

TABLE 1: Parameters Obtained by the Global Fitting Analysis of the DTAC/Water System Compressibilities

$v_{W(B)}^{\circ}$ Å^3	$\beta_{W(B)}^{\circ}$ 10^{-5} bar^{-1}	$\eta_{W(B)}$	β_L° 10^{-5} bar^{-1}	η_L	N	ΔG° kcal mol^{-1}
29.89 ± 0.01	1.105 ± 0.001	130 ± 10	5.27 ± 0.02	16.5 ± 0.1	11.7 ± 0.2	-9.5 ± 0.2

function of pressure. The general behavior described by the previous analysis is confirmed: bound water has a very low compressibility, while the lipid β value strongly depends on pressure. Moreover, a series of information on the hydration properties of DTAC is derived. Figure 10 shows the concentration and pressure dependence of the average hydration number $\langle j \rangle$. $\langle j \rangle$ increases as a function of the sample water concentration but remains constant below $c = 0.6$, suggesting that at this concentration a full hydration condition is achieved. By contrast, $\langle j \rangle$ does not vary during compression. Then, DTAC hydration is independent of pressure, and as a consequence, also the α_j distribution (i.e., the fraction of lipid molecules directly interacting with j water molecules) should only depend on sample concentration. In Figure 11, α_j is shown in the form of histograms at four different concentrations: large changes in the distribution of the hydration water are detected in the different experimental conditions.

D. Molecular Parameters. As the pressure dependence of the sample volume composition has been established, lipid and aqueous volumes can be calculated at each pressure from unit cell data. Considering the size and shape of the structure elements in the different lipid phases, a series of molecular parameters can be derived as a function of pressure following a well-known procedure.[14]

We should recall here that the structure of the *Ia3d* cubic phase consists of 24 identical, straight hydrocarbon rods of circular cross section, joined together 3×3. The volume (V_{par}) and the surface area (S_{par}) of each hydrocarbon rod can be written[14]
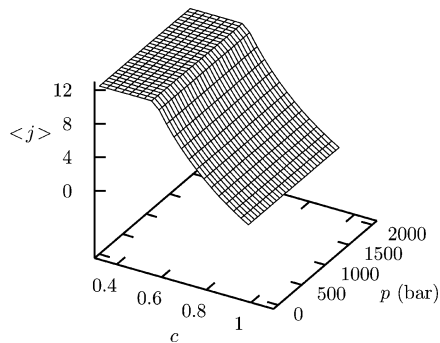
$$V_{par} = \pi r^2 l (1 - k_v r/l) \tag{14}$$

$$S_{par} = 2\pi r l (1 - k_s r/l) \tag{15}$$

where l and r are the length ($l = a\sqrt{8}$) and radius of the rod, respectively, and $k_v = 0.491$ and $k_s = 0.735$ are geometrical constants related to the bevel-shaped ends of the rod. As the volume of each hydrocarbon rod can also be expressed by

$$V_{par} = (V\phi_L v_{par}/v_L)/24 \tag{16}$$

where v_{par} is the volume of the DTAC hydrocarbon chain (which we assume to feature the same pressure dependence of v_L), the rod radius can be derived by combining eqs 14 and 16. From eq 15, the average area per molecule at the

polar/apolar interface (s_{par}) can be calculated

$$s_{par} = S_{par} 24/n_L \tag{17}$$

In the hexagonal phase, the radius of the cylinder and the average area available to one molecule at the polar/apolar interface can be determined by using (see Definitions and Abbreviations)

$$r = [(\sigma\phi_L v_{par}/v_L)/\pi]^{1/2} \tag{18}$$

$$s_{par} = 2\pi r l / n_L \tag{19}$$

For the *Pm3n* micellar cubic phase, a simple geometric approach cannot be used, as the precise shape of the micelles is unknown. However, the volumes of the hydrocarbon micelles in the DTAC system and the S_{par}/V_{par} ratio have been reported by Vargas et al. for a sample at $\phi_L = 0.52$ ($a = 85.4$ Å) at ambient pressure:[15] The volumes of the micelles in the **a** and **c** positions, measured from electron density maps, were $V_{a,par} = 25.1 \times 10^3$ Å^3 and $V_{c,par} = 28.6 \times 10^3$ Å^3, while it resulted in $S_{a,par} = 0.149 V_{a,par}$ and $S_{c,par} = 0.157 V_{c,par}$. Assuming a direct
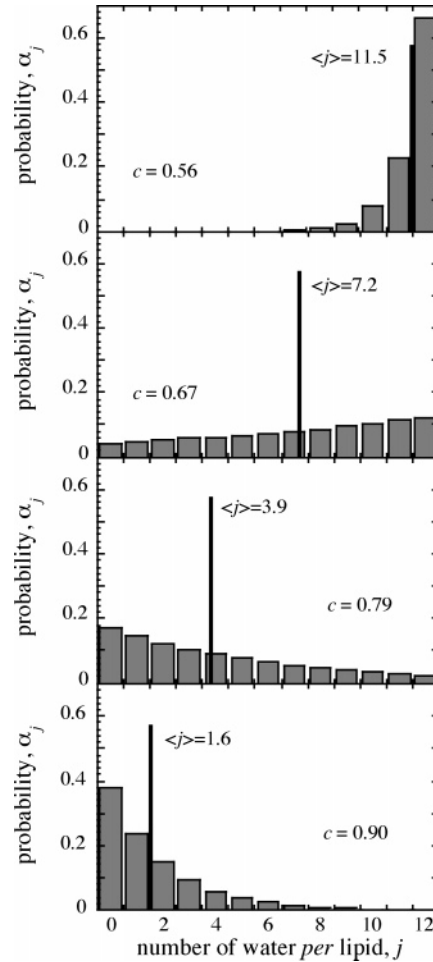
Figure 11. Distribution of the hydration water molecules on the DTAC molecules at four different sample concentrations. j is the number of water molecules per lipid; α_j gives the fraction of lipid molecules directly interacting with the j water molecules. The corresponding average hydration number, $\langle j \rangle$, is also reported.

Figure 10. Concentration and pressure dependence of the DTAC average hydration number, $\langle j \rangle$.
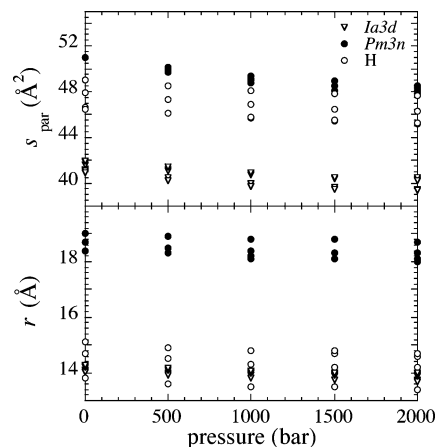
Figure 12. Pressure dependence of the hydrocarbon radius, r, and of the cross-sectional area per molecule at the polar/apolar interface, s_{par}, of the *Pm3n*, H, and *Ia3d* phases for DTAC samples at 25 °C at different concentrations.

relationship between the micelle volumes and the volume of the unit cell, the average area per molecule at the polar/apolar interface can be then calculated at any pressure for each concentration. However, the shape of the micelles is not described in details; thus, an estimate of the length of the hydrocarbon chain has been obtained by considering micelles of spherical form.

The structural parameters calculated using the pressure-dependent volume concentrations derived in the previous paragraph are shown in Figure 12. The behavior observed in the three different phases is rather similar: both the average area per molecule at the polar/apolar interface and the hydrocarbon chain length decrease during compression. The variations are nevertheless small and confirm that the conformational changes induced by pressure in the DTAC molecule are surprisingly small, in contrast with the results obtained for inverse lipid phases.[6,9] Moreover, it should be emphasized that at any pressure the area per molecule is found to increase versus water concentration (i.e., as a function of hydration). In a contrary manner, the area per molecule at constant concentration slightly decreases during compression, indicating that pressure induces some contraction of the polar surfaces.

IV. Discussion

Soft-matter macromolecular systems include proteins, biomembranes, surfactant, lipid, and block copolymer mesophases, cellular cytoskeletal networks, and other large-molecule assemblies found in living systems. Molecules in these systems may have a huge number of conformational substates. The free energies of different substates often differ only slightly, even though the 3D molecular structures may differ greatly. Pressures in the range of up to several kilobars alter the ensemble of conformational substates in a macromolecular assembly: since the ensemble of conformational substates under a given set of environmental conditions greatly determines functional activity for many such systems (e.g., proteins, biomembranes), it follows that medium pressure affects biological function.[1,3]

Thus, medium pressure structural studies are topical and ripe for exploration. In this context, the study of lipid−water dispersions is particularly relevant, as it concerns not only the physical chemistry and the mechanical properties of the assembly, but also the functional characteristics of cell membranes. Under compression, lipids adapt to volume restriction by changing their conformation and packing. Since a delicate

balance of competing energetic contributions is involved in stabilization of lipid phases in water, such small changes in conformation can determine large structural transformations and reveal interesting and unusual features.

For lipid inverse systems, remarkable structural effects have been described (as a negative phase compressibility, a large increase of the lipid hydration level in excess of water, and a series of phase transitions[4,6,9]), and a strong pressure dependence of the basic geometrical shape of the lipid molecules forming type II structures has been reported.[6,8,9] Intermediate pressure should affect the structural properties of direct phases in a different way, owing to their different topology. However, only a few studies have been performed on such systems:[11,12] the main results concerned the phase transition from rodlike micelles to lamellar phases observed in concentrated micellar systems and microemulsions.[12]

In the present case, the high-pressure lyotropic behavior of the DTAC/water system has been considered. DTAC shows an extended direct polymorphism, forming at ambient pressure and as a function of hydration a lamellar, a bicontinuous *Ia3d* cubic, a hexagonal, and a micellar *Pm3n* cubic phase (see Figure 1). Compression has been found to induce phase transitions from the hexagonal to the micellar *Pm3n* cubic phase and from the bicontinuous *Ia3d* cubic to the hexagonal phase. As expected, the pressure at which transition occurs depends on the lipid concentration (see Figure 4). Under highly dehydrated conditions, the formation of a lamellar phase at high pressure has been observed. A lamellar phase also forms transitorily during the phase transition from the *Ia3d* cubic to the hexagonal phase. The presence of this phase seems to indicate that changes in local phase concentration occur during the transition. As a consequence, a less hydrated lamellar phase in equilibrium with a more hydrated hexagonal phase forms. According to this hypothesis, after the disappearance of the *Ia3d* cubic phase, only the hexagonal phase still exists.

Phase isothermal compressibilities β have been calculated from unit cell dimensions (Figures 7 and 8). The coefficients of the isothermal compressibility in the three lipid phases are found to be positive: they decrease by increasing the pressure and continuously increase with lipid concentration, even when phase boundaries are crossed. Moreover, β values are systematically lower than those of bulk water (Figures 7 and 8). Owing to the differences in hydrogen bond network in confined spaces, it is clear that water within the lipid phase exhibits a lower compressibility than in the bulk. The calculated partial molecular values (see the fitted values in Figure 9) confirm that bound water compressibility is unusually low (about 3 to 10 times lower than the compressibility observed in the bulk), while indicating for DTAC a compressibility very dependent on pressure. As lipid compressibility represents a measure of intermolecular interactions, the observed behavior should reflect the tightness of intrinsic hydrocarbon packing induced by pressure, but also accounts for the presence of interstitial volumes resulting from interactions of the solute with the solvent.

Considering that in the more hydrated conditions only a fraction of water in the aqueous compartment can strongly interact with the lipid surface, a simple thermodynamic model has been formulated to extract from the partial compressibility of water the contribution of the "bound" water as well as the contribution of water molecules which basically behave as "bulk" water. A series of prominent findings, which can be relevant to model the characteristic of the hydration shell in many biological systems, have emerged form this analysis. First, the maximum hydration number N for the DTAC is 12 (see

Table 1 and Figure 10). Above this limit, excess water inside the lipid phase exhibits the basic properties of bulk water. Second, the $\Delta G°$ value (which is related to the work required to hydrate the hydrophilic DTAC surfaces) corresponds to the strength of the stronger hydrogen bonds, which usually lie between 2 and 10 kcal mol^{-1}. Third, the average hydration number, $\langle j \rangle$, shows that hydration is independent of pressure, even at the higher investigated concentrations (see Figure 10). Fourth, in full hydration conditions, lipid molecules share an equal number of water molecules, while in less hydrated conditions, a wide distribution of water molecules per lipid is found (see the distribution of the hydration water molecules on the DTAC polar head, α_j, shown in Figure 11). Indeed, more than 30% of the lipid molecules were unhydrated in the drier samples. This result can be relevant to account for lipid phase diagrams obtained in the less hydrated conditions.

The molecular parameters of DTAC in the different phases have then been determined as a function of pressure (see Figure 12). From data, it is evident that intermediate pressures induce only small conformational changes, unlike the large changes observed in lipid molecules forming type II structures. In particular, during compression, both the area per molecule, s_{par}, and the length of the hydrocarbon chain, r, reduce in a tiny but continuous way. However, as the changes of the area per molecule under compression do not correspond to a decrease of the hydration number, it can be suggested that the ordering of water molecules in close vicinity of the smooth polar surfaces also involves the second and/or third hydration layers. This would result in stabilization of the more hydrated structures at high pressures. Accordingly, high-pressure data show that the *Pm3n* is favored with respect to the H phase at larger hydration, while the H is favored with respect to the *Ia3d* phase in less hydrated conditions.

In conclusion, this work shows that a better understanding of the mesomorphism of lipid phases can be reached by analyzing the relationship between the lipid molecular structure and a few thermodynamic parameters when pressure and concentration vary. The present analysis is rather limited, but the reported experimental data could help to put forward different mechanisms and analysis in further theoretical approaches.

Definitions and Abbreviations

L and W, symbols for DTAC and water molecules.

c, weight fraction of DTAC in the mixture.

ν_W and ν_L, nominal specific volumes of water and DTAC molecules at ambient pressure, respectively.

ϕ_i, volume concentration of the ith species in the mixture; nominally, the DTAC volume concentration at ambient pressure is $\phi_L = c\nu_L/[c\nu_L + (1-c)\nu_W]$.

a, unit cell dimension in the hexagonal and cubic phases

d, unit cell dimension in the one-dimensional (1D) lamellar phase.

V, volume of the unit cell; in the cubic phase, $V = a^3$; in the hexagonal phase, $V = \sigma \ell$, where ℓ is the height of the hexagonal cell, considered infinite, and $\sigma = a^2\sqrt{3}/2$ is the area the hexagonal primitive two-dimensional (2D) unit cell.

$V_i = \phi_i V$, volume of the unit cell region occupied by the ith species in the mixture; ν_i, molecular volume of the ith species in the mixture.

$n_i = V_i/\nu_i$, number of molecules of the ith species in the unit cell volume V. By definition, $V = \Sigma_i n_i \nu_i$.

$\beta_{3D} = -V^{-1}(\partial V/\partial p)_T$, coefficient of 3D isothermal compressibility.

$\beta_{2D} = -\sigma^{-1}(\partial\sigma/\partial p)_T$, coefficient of 2D isothermal compressibility.

$\beta_i = -V_i^{-1}(\partial V_i/\partial p)_T$, coefficient of isothermal partial compressibility of the ith species in the mixture. By definition, it coincides with the isothermal partial molecular compressibility of the ith species, $\beta_i = -\nu_i^{-1}(\partial \nu_i/\partial p)_T$.

$\eta_i = (\partial\beta_i^{-1}/\partial p)_{p=0}$, first derivative of the reciprocal isothermal partial compressibility (the so-called isothermal bulk modulus) of the ith species at zero pressure.

χ, volume fraction of water molecules hardly bound to the DTAC polar surfaces with respect to the total water in the unit cell volume.

References and Notes

(1) Winter, R. Synchrotron X-ray and neutron small-angle scattering of lyotropic lipid mesophases, model biomembranes and proteins in solution at high pressure. *Biochim. Biophys. Acta* **2002**, *1595*, 160−184.

(2) Winter, R. Effects of hydrostatic pressure on lipid and surfactant phases. *Curr. Opin. Colloid Interface Sci.* **2001**, *6*, 303−312.

(3) Gruner, S. M. Soft materials and biomaterials under pressure. In *High-Pressure Crystallography*; Katrusiak, A., McMillian, P. Eds.; NATO Science Series; Kluwer Academic Publishers: Dordrecht, The Netherlands, 2004; pp 543−556.

(4) So, P. T. C.; Gruner, S. M.; Erramilli, S. Pressure-induced topological phase transitions in membranes. *Phys. Rev. Lett.* **1993**, *70*, 3455−3458.

(5) Winter, R.; Czeslik, C. Pressure effects on the structure of lyotropic lipid mesophases and model biomembrane systems. *Z. Kristallogr.* **2000**, *215*, 454−474.

(6) Pisani, M.; Narayanan, T.; Di Gregorio, G.; Ferrero, C.; Finet, S.; Mariani, P. Compressing inverse lyotropic systems: structural behavior and energetics of dioleoyl phosphatidyl ethanolamine. *Phys. Rev. E* **2003**, *68*, 21924−21934.

(7) Czeslik, C.; Winter, R.; Rapp, G.; Bartels, K. The temperature and pressure dependent phase behavior of the monoacylglycerides monoolein and monoelaidin. *Biophys. J.* **1995**, *68*, 1423−1429.

(8) Mariani, P.; Paci, B.; Bosecke, P.; Ferrero, C.; Lorenzen, M.; Caciuffo, R. The effects of hydrostatic pressure on the monoolein-water system: an estimate of the energy function of the inverted *Ia3d* cubic phase. *Phys. Rev. E* **1996**, *54*, 5840−5843.

(9) Pisani, M.; Bernstorff, S.; Ferrero, C.; Mariani, P. Pressure induced cubic-to-cubic phase transition in monoolein hydrated system. *J. Phys. Chem. B* **2001**, *105*, 3109−3119.

(10) Winter, R.; Erbes, J.; Czeslik, C.; Gabke, A. Effect of pressure on the stability, phase behavior and transformation kinetics between structures of lyotropic lipid mesophases and model membrane systems. *J. Phys. Condens. Matter* **1998**, *10*, 11499−11518.

(11) Lesemann, M.; Thirumoorthy, K.; Kim, Y. J.; Jonas, J.; Paulaitis, M. E. Pressure dependence of the critical micelle concentration of a nonionic surfactant in water studied by ^{1}H-NMR. *Langmuir* **1998**, *14*, 5339−5341.

(12) Seto, H.; Okuhara, D.; Kawabata, Y.; Takeda, T.; Nagao, M.; Suzuki, J.; Kamikubo, H.; Amemiya, Y. Pressure and temperature effects on the phase transition from a dense droplet to a lamellar structure in a ternary microemulsion. *J. Chem. Phys.* **2000**, *112*, 10608−10614.

(13) Balmbra, R. R.; Clunie, J. R.; Goodman, J. F. *Nature (London)* **1969**, *222*, 1159−1160.

(14) Mariani, P.; Luzzati, V.; Belacroix, H. Cubic phases of lipid-containing systems. Structure analysis and biological implications. *J. Mol. Biol.* **1988**, *204*, 165−189.

(15) Vargas, R.; Mariani, P.; Gulik, A.; Luzzati, V. Cubic phases of lipid containing systems. The structure of phase Q223 (space group *Pm3n*). An x-ray scattering study. *J. Mol. Biol.* **1992**, *225*, 137−145.

(16) Luzzati, V.; Vargas, R.; Mariani, P.; Gulik, A.; Delacroix, H. Cubic phase of lipid-containing systems. Element of a theory and biological connotations. *J. Mol. Biol.* **1993**, *229*, 540−551.

(17) Luzzati, V. X-ray diffraction studies of lipid-water systems. In *Biological Membranes*; Chapman, D., Ed.; Academic Press: London, 1968; pp 1−60.

(18) Macdonald, J. R. Review of some experimental and analytical equations of state. *Rev. Mod. Phys.* **1969**, *41*, 316−349.

(19) Svergun, D. I.; Richard, S.; Koch, M. H. J.; Sayers, Z.; Kuprin, S.; Zaccai, G. Protein hydration in solution: experimental observation by X-ray and neutron scattering. *Proc. Natl. Acad. Sci. U.S.A.* **1998**, *95*, 2267−2272.

(20) Israelachvili, J. N. *Intermolecular and Surface Forces*; Academic Press: London, 1992.

(21) Taulier, N.; Chalikian, T. V. Compressibility of protein transitions. *Biochim. Biophys. Acta* **2002**, *1595*, 48−70.

(22) Hayward, A. T. J. Compressibility equations for liquids: a comparative study. *Br. J. Appl. Phys.* **1967**, *18*, 965−977.